Article

A Satellite-Based Model for Simulating Ecosystem Respiration in the Tibetan and Inner Mongolian Grasslands

Rong Ge [1,2] **, Honglin He** [1,3,*] **, Xiaoli Ren** [1,*] **, Li Zhang** [1,3] **, Pan Li** [4] **, Na Zeng** [1,2] **, Guirui Yu** [1,3] **, Liyun Zhang** [1,2] **, Shi-Yong Yu** [5] **, Fawei Zhang** [6] **, Hongqin Li** [6] **, Peili Shi** [1] **, Shiping Chen** [7] **, Yanfen Wang** [2] **, Xiaoping Xin** [8] **, Yaoming Ma** [2,9,10] **, Mingguo Ma** [11] **, Yu Zhang** [12] **and Mingyuan Du** [13]

[1] Key Laboratory of Ecosystem Network Observation and Modeling, Institute of Geographic Sciences and Natural Resources Research, Chinese Academy of Sciences, Beijing 100101, China; ge7218@163.com (R.G.); li.zhang@igsnrr.ac.cn (L.Z.); zengna900110@163.com (N.Z.); yugr@igsnrr.ac.cn (G.Y.); ciwei659454714@126.com (L.Z.); shipl@igsnrr.ac.cn (P.S.)

[2] University of Chinese Academy of Sciences, Beijing 100049, China; yfwang@gucas.ac.cn

[3] College of Resources and Environment, University of Chinese Academy of Sciences, Beijing 100049, China

[4] State Key Laboratory of Environmental Geochemistry, Institute of Geochemistry, Chinese Academy of Sciences, Guiyang 550002, China; ncepulee@126.com

[5] School of Geography, Geomatics, and Planning, Jiangsu Normal University, Xuzhou 221116, China; syu@jsnu.edu.cn

[6] Northwest Plateau Institute of Biology, Chinese Academy of Sciences, Xining 810001, China; mywing963@126.com (F.Z.); lihongqin_00@126.com (H.L.)

[7] State Key Laboratory of Vegetation and Environmental Change, Institute of Botany, Chinese Academy of Sciences, Beijing 100093, China; spchen@ibcas.ac.cn

[8] Institute of Agricultural Resources and Regional Planning, Chinese Academy of Agricultural Sciences, Beijing 100081, China; xinxiaoping@caas.cn

[9] Key Laboratory of Tibetan Environment Changes and Land Surface Processes, Institute of Tibetan Plateau Research, Chinese Academy of Sciences, Beijing 100101, China; ymma@itpcas.ac.cn

[10] CAS center for Excellence in Tibetan Plateau Earth Science, Chinese Academy of Sciences, Beijing 100101, China

[11] Chongqing Engineering Research Center for Remote Sensing Big Data Application, School of Geographical Sciences, Southwest University, Chongqing 400715, China; mmg@swu.edu.cn

[12] Northwest Institute of Eco-Environment and Resources, Chinese Academy of Sciences, Lanzhou 730000, China; yuzhang@lzb.ac.cn

[13] Institute for Agro-Environmental Sciences, National Agriculture and Food Research Organization, Tsukuba, Ibaraki 3058604, Japan; dumy@affrc.go.jp

* Correspondence: hehl@igsnrr.ac.cn (H.H.); renxl@igsnrr.ac.cn (X.R.); Tel.: +86-10-6488-9599 (H.H.); +86-10-6488-9851 (X.R.)

Abstract: It is important to accurately evaluate ecosystem respiration (*RE*) in the alpine grasslands of the Tibetan Plateau and the temperate grasslands of the Inner Mongolian Plateau, as it serves as a sensitivity indicator of regional and global carbon cycles. Here, we combined flux measurements taken between 2003 and 2013 from 16 grassland sites across northern China and the corresponding MODIS land surface temperature (*LST*), enhanced vegetation index (*EVI*), and land surface water index (*LSWI*) to build a satellite-based model to estimate *RE* at a regional scale. First, the dependencies of both spatial and temporal variations of *RE* on these biotic and climatic factors were examined explicitly. We found that plant productivity and moisture, but not temperature, can best explain the spatial pattern of *RE* in northern China's grasslands; while temperature plays a major role in regulating the temporal variability of *RE* in the alpine grasslands, and moisture is equally as

important as temperature in the temperate grasslands. However, the moisture effect on *RE* and the explicit representation of spatial variation process are often lacking in most of the existing satellite-based *RE* models. On this basis, we developed a model by comprehensively considering moisture, temperature, and productivity effects on both temporal and spatial processes of *RE*, and then, we evaluated the model performance. Our results showed that the model well explained the observed *RE* in both the alpine (R^2 = 0.79, RMSE = 0.77 g C m^{-2} day^{-1}) and temperate grasslands (R^2 = 0.75, RMSE = 0.60 g C m^{-2} day^{-1}). The inclusion of the *LSWI* as the water-limiting factor substantially improved the model performance in arid and semi-arid ecosystems, and the spatialized basal respiration rate as an indicator for spatial variation largely determined the regional pattern of *RE*. Finally, the model accurately reproduced the seasonal and inter-annual variations and spatial variability of *RE*, and it avoided overestimating *RE* in water-limited regions compared to the popular process-based model. These findings provide a better understanding of the biotic and climatic controls over spatiotemporal patterns of *RE* for two typical grasslands and a new alternative up-scaling method for large-scale *RE* evaluation in grassland ecosystems.

---

1. Introduction

Grasslands are one of the most widespread vegetation types and store one-fifth of the total global carbon in its vegetation and soil [1,2]; thus, they play an important role in the global carbon cycle. The extensive grasslands in China make up ~10% of the total area of grasslands in the world and have been estimated to store 9–15% of the total carbon held in the grasslands worldwide [3]. Northern China's grasslands located in the Tibetan Plateau and Inner Mongolian Plateau, in particular, constitute the majority (more than 70%) of the grasslands in China and represent two significant grassland types worldwide (i.e., alpine and temperate grasslands) [4]. Moreover, they are sensitive to climate changes due to their unique plateau topography, the extreme cold, arid and semi-arid ecological environment and the high soil carbon density [5–7]. Therefore, a better understanding of the carbon cycle in northern China's grasslands is necessary for it to serve as a sensitivity indicator of regional and global carbon cycles.

Ecosystem respiration (RE) is an important outflow component of ecosystem carbon cycle and represents the second largest carbon exchanges between terrestrial ecosystems and the atmosphere [8]. However, as the result of the complex interactions among physical, chemical, and biological processes, *RE* varies greatly at different temporal and spatial scales [9]. Extensive studies at regional or global scales suggest that *RE* estimates still remains a large uncertainty [10]. Therefore, it is particularly essential but challenging to accurately evaluate the regional *RE* in northern China's grasslands for a quantitative assessment of the terrestrial ecosystem carbon budget and its response to future climate changes.

Generally, modeling is the commonly adopted method for inferring *RE* at a large scale. Remote-sensing models, with relatively simple model structures and high spatiotemporal resolutions, provide promising tools for monitoring regional *RE*. Currently, with the development of fine-scale remote-sensing technology and long-term regional and global FLUXNET observations, extensive studies have revealed the robust statistical and physiologically meaningful relationships between *RE* and satellite products, e.g., the land surface temperature (*LST*) [11–13] and vegetation index (VI) [14–16]. Based on this information, many semi-empirical satellite-based models were developed and well validated at the plot scale [13,16–19]. However, *RE* at large scale involves complex spatial and temporal variation processes [20]. Few satellite-based models have an explicit representation of the spatial process of RE. Specifically, the basal respiration rate, an important parameter in *RE*

models to describe the location-specific respiration rate, is usually set as a constant parameter, which introduces considerable error in the simulated spatial variability of *RE* [8,20,21]. Therefore, it is critical to identify the controlling mechanism involved in the spatial variations of *RE* with more comprehensive data, not just in the temporal variations, thus serving as a valuable basis to better understand patterns of *RE* at regional scale and to scale-up from specific sites to vegetation biomes. In addition, both climatic and biotic controls over *RE* should be considered comprehensively in *RE* simulation [22,23]. In satellite based models, *RE* has often been linked to temperature or plant productively solely. Some studies advanced *RE* estimates by accounting for the combined two effects of temperature and plant productivity [13,15]. The moisture limitation on *RE* is often lacking in most of the current satellite-based respiration models, leading to a potential underestimation of drought effects on respiration (e.g., [19,24]). However, grasslands are one of the most sensitive ecosystems to the alteration of water regimes [25]. Water stress was found to have a strong influence on northern China's grasslands, especially in southwestern Inner Mongolia and northwestern Tibet [26]. Recently, some satellite-based models gradually began incorporating the moisture effect on RE, but it still depends which satellite product and form are selected to represent the moisture factor and the response process of *RE* to moisture. For instance, a linear equation of an indirect water indicator (diurnal *LST* difference, LST_{diff}) was utilized in the RECO model during the dry season for water-limited biomes, which were mostly concentrated in the Mediterranean climate region without a temperature limitation [27]; thus, its utility in northern China's grasslands still needs to be validated. Root-zone soil moisture derived from the Advanced Microwave Scanning Radiometer-Eos was adopted in a soil respiration (Rs) model in the Midwest USA, and it yielded a lower explanation capacity for seasonal variation of Rs than the surface soil moisture under extreme moisture regimes [28]. Currently, increasing attention is being given to the moisture effect on *RE* [29,30], as most climate change scenario analyses have predicted that the frequency and severity of drought will increase in most biomes across the world [31]. It is practical to develop a satellite-based *RE* model that integrates temperature, plant productivity, and moisture effects together in both temporal and spatial processes, to yield reliable simulations of regional *RE* for northern China's grasslands.

This study was based on 57 site-year flux-tower data and remote-sensing data from northern China's grasslands. The major objectives of this study were threefold: (i) to quantify the relationships of climatic and biotic factors and the spatial and temporal variability of *RE* in the Tibetan alpine grasslands and the Inner Mongolian temperate grasslands; (ii) to develop a high-resolution satellite-based model for simulating *RE* at regional scale on the basis of comprehensive consideration of vegetation productivity, temperature, and moisture; and (iii) to assess the model performance in terms of the temporal dynamics as well as the spatial pattern simulation of *RE* in northern China's grasslands.

2. Materials and Methods

2.1. Study Area

This study was conducted in the alpine grasslands on the Tibetan Plateau and the temperate grasslands on the Inner Mongolian Plateau. The Tibetan region is in the alpine climate zone, where temperature appears as the controlling factor for the grassland ecosystems. With an average elevation of ca. 4000 m, the mean annual air temperature on the plateau ranges between −5.75 and 2.57 °C, and the mean annual precipitation varies from 200 to 600 mm. The alpine meadow covers more than half of the plateau, representing not only a typical ecosystem in central Asia alpine environment but also a unique ecosystem within the alpine regions of the world [32]. Located in the arid and semi-arid zone, the grassland ecosystems in the Inner Mongolian region are mainly limited by moisture. With an average elevation ca. 1000 m, the mean annual temperature in this area varies between 3 and 6 °C, and the mean annual precipitation ranges from 200 to 350 mm. The temperate grasslands are a typical vegetation type under the temperate continental climate and they represent an important component of the Eurasian grasslands [33]. According to the Atlas of China's Grassland Resources

(1:1,000,000), we fully considered the spatial representativeness of the flux-tower sites collected for this research and focused on three types: (i) alpine meadow; (ii) alpine meadow steppe (AS); and (iii) temperate steppe. The alpine meadow was further subdivided into three types: (1) alpine *Kobresia* meadow (KO); (2) alpine shrub meadow (SH); and (3) alpine swamp meadow (SW); the temperate steppe was also subdivided into three types: (1) meadow steppe (MS); (2) typical steppe (TS); (3) and desert steppe (DS). The distribution of these vegetation functional types (PFTs) as well as the typical grassland flux-tower sites is shown in Figure 1.
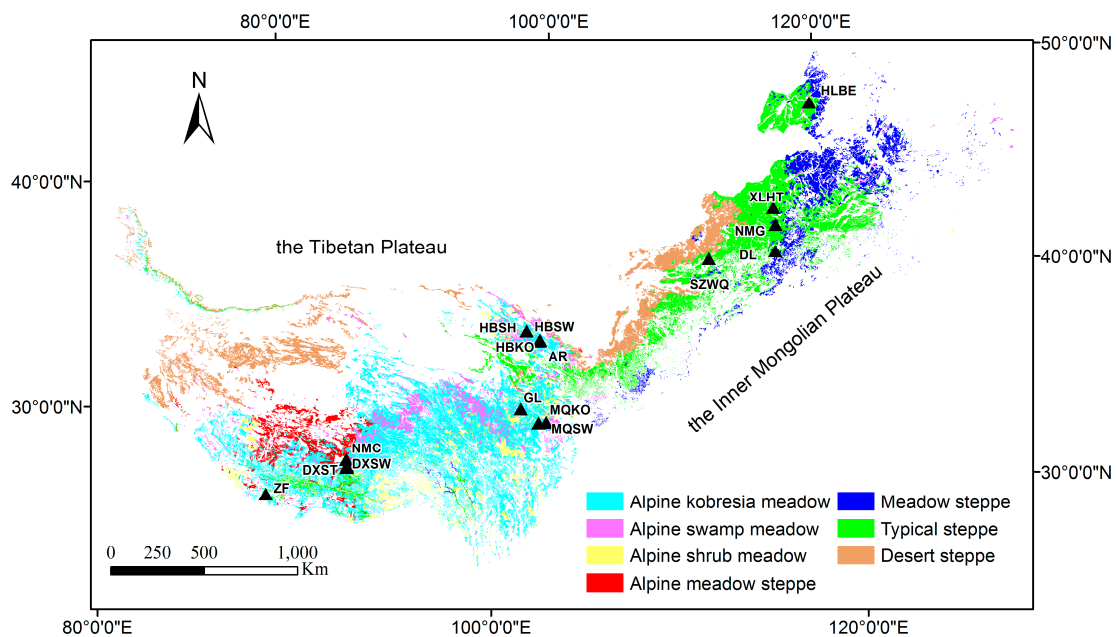

Figure 1. Map showing the spatial distribution of the alpine and temperate grasslands in China. Triangles denote the 16 flux-tower sites. DXST = DangXiong alpine meadow steppe; DXSW = DangXiong alpine swamp meadow; HBSW = HaiBei alpine swamp meadow; HBSH = HaiBei alpine shrub meadow; HBKO = HaiBei alpine *Kobresia* meadow; MQSW = MaQu alpine swamp meadow; MQKO = MaQu alpine *Kobresia* meadow; ZF = ZhuFeng; NMC = NaMuCuo; GL = GuoLuo; AR = ARou; NMG = NeiMengGu; XLHT = XiLinHaoTe; SZWQ = SiZiWangQi; HLBE = HuLunBeEr; DL = DuoLun.

2.2. Data

2.2.1. Flux-Tower Data

A total of 57 site-year data from 16 grassland sites during 2003–2013 were retrieved from the ChinaFLUX and the Coordinated Observations and Integrated Research over Arid and Semi-Arid China (COIAS) databases, including 43 site-years from 11 sites on the Tibetan Plateau and 14 site-years from 5 sites on the Inner Mongolia Plateau (Table 1). The observed eddy-covariance data were processed through a three-dimensional coordinate rotation, WPL (Webb-Pearman-Leuning) correction, and invalid data exclusion [34]. Subsequently, the missing nighttime *RE* and daytime *RE* data were calculated using the Lloyd-Taylor equation based on net ecosystem exchange (NEE) observations during the nighttime [35]. The entire procedure was completed using the ChinaFLUX CO_2 data processing system [36]. The half-hourly flux data was summed to obtain daily values, and the site-years with more than 30% of the daily *RE* missing were eliminated. To comply with the temporal scale of the Moderate Resolution Imaging Spectroradiometer (MODIS) 8-day composite imagery, the processed daily *RE* were averaged within the same periods.

Table 1. Main characteristics of the 16 flux-tower sites over China's grasslands.

Grassland Type	Site Name	Location	Elevation (m)	Canopy Height (m)	Tower Height (m)	Operation Period
Alpine shrub meadow	HBSH	37.67°N 101.33°E	3293	0.6–0.7	2.2	2003–2008, 2010–2012
Alpine *Kobresia* meadow	HBKO	37.61°N 101.31°E	3148	0.2–0.3	2.2	2003–2005, 2009, 2012
	GL	34.35°N 100.56°E	3980	0.2–0.3	2.2	2007, 2010–2011, 2013
	AR	38.04°N 100.46°E	3033	0.2–0.3	3.15	2008–2010
	MQKO	33.88°N 102.15°E	3533	0.2–0.3	3.15	2009–2010
Alpine swamp meadow	HBSW	37.61°N 101.33°E	3160	0.2–0.5	2.2	2004–2008, 2010–2012
	DXSW	30.47°N 91.06°E	4286	0.2–0.5	2.1	2009–2010
	MQSW	33.76°N 101.68°E	3503	0.3–0.5	3.2	2010
Alpine meadow steppe	DXST	30.50°N 91.06°E	4333	<0.2	2.2	2004–2010
	ZF	28.36°N 86.95°E	4293	<0.2	3.1	2009
	NMC	30.77°N 90.96°E	4730	<0.2	3.1	2009
Typical steppe	NMG	43.53°N 116.67°E	1200	0.2–0.3	4	2004–2008, 2010, 2012
	DL	42.05°N 116.28°E	1324	0.3–0.5	5	2010–2011
	XLHT	44.13°N 116.32°E	1187	0.1–0.3	5	2010–2011
Desert steppe	SZWQ	41.8°N 111.9°E	1438	0.1–0.2	3	2011–2012
Meadow steppe	HLBE	49.06°N 119.4°E	628	0.3–0.5	3	2012

2.2.2. Remote-Sensing Data

At the site scale, the MODIS products of the *LST*, enhanced vegetation index (*EVI*), and land surface water index (*LSWI*) at each site-year (2003–2013) were downloaded from the University of Oklahoma Data Center (http://www.eomf.ou.edu/visualization/manual/), based on the pixels where the flux towers located, to match up with the flux data for model parametrization.

At the spatial scale, the 8-day (best observation in 8 days) MODIS land surface reflectance datasets (MOD09A1, Level 3, Collection 5) during 2001–2010 were downloaded from NASA Land Processes Distributed Active Archive Center (https://lpdaac.usgs.gov/) to generate the spatial *EVI* and *LSWI* data using Equations (1) and (2), as model drivers in regional simulation.

$$EVI = G \times (\rho_{nir} - \rho_{red})/(\rho_{nir} + (C_1 \times \rho_{red} - C_2 \times \rho_{blue}) + L), \tag{1}$$

$$LSWI = (\rho_{nir} - \rho_{swir}) / (\rho_{nir} + \rho_{swir}), \tag{2}$$

where ρ_{nir}, ρ_{red}, ρ_{blue}, and ρ_{swir} represent the reflectance of near infrared bands (NIR, 841–875 nm), red bands (620–670 nm), blue bands (459–478 nm), and short wave infrared bands (SWIR, 1628–1652 nm), respectively. The coefficients G, C_1, C_2 and L used in the *EVI* algorithm are 2.5, 6, 7.5 and 1, respectively [37].

The MOD11A2 and MYD11A2 products (Level 3, Collection 5), which are 8-day average values of cloud free observations, were also downloaded from the LP DAAC data pool to obtain the spatial daytime *LST* and nighttime *LST* data, respectively. The spatial resolution of *EVI* and *LSWI* is 500 m, and that of *LST* is 1 km. For the regional application in China's grasslands, the extracted *EVI* and *LSWI* were resampled to a 1-km resolution. The temporal resolution of these products is 8-day, which ensures a better data quality as selected on the basis of the absence of clouds or aerosol, etc., and is confirmed by extensive *RE* modeling research to be able to robustly capture the seasonal variation of *RE* [24,27,28]. Additionally, to further reduce the effect of cloud and to capture the seasonality of *EVI*, the original time series were smoothed using the double logistic curve fit in the TIMESAT software (Lund University, Lund, Sweden) [38].

2.3. Model

RE at the regional scale is a coupling result of complex spatial and temporal processes. The process of spatial variability refers to the basic trend of *RE* changing with the climate and substrate at a specific location, which is especially significant in regional simulations [39]; the process of temporal variability refers to the cyclical changes of *RE* induced by the seasonal dynamics of environmental factors and plant growth. A multiplication factor is usually used to express the interaction of the above two processes in an *RE* simulation [20–22,27]. Based on the remote-sensing model RECO [27] and the traditional climate-driven model T&P [20,22], we put forward a modified model of *RE* for grasslands by taking the effects of temperature, vegetation productivity, and moisture on both the spatial and temporal variability of *RE* into account and making full use of the high-resolution satellite data as the model drivers. To account for spatial and temporal variability separately, we partition *RE* into a site-specific reference respiration rate (*Reref*) and the remaining seasonal variation (*f(T,P,W)*), which is detrended for site characteristics (Equation (3)). The structure of the model is shown below (Figure 2).
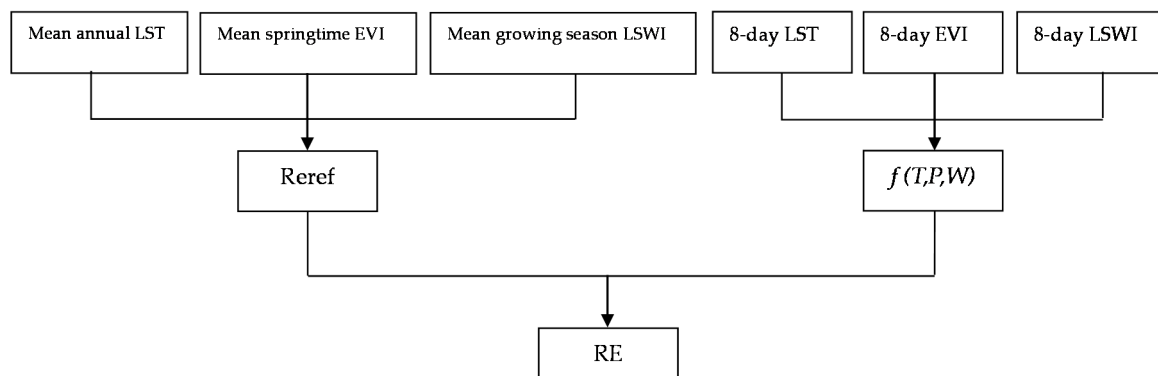
$$RE = Reref * f\ (T,\ P,\ W), \tag{3}$$

Figure 2. Structure of the ecosystem respiration (*RE*) model for grasslands.

2.3.1. Representation of Spatial Variability of *RE*

Reref is the site-specific respiration rate at the reference temperature (*Tref*). It is used to describe the difference in basal respiration between sites and years, thereby reflecting the spatial variability of *RE* [8]. Numerous studies have indicated that a spatially heterogeneous *Reref* results in a better estimation of *RE* at different sites [20–22,27]. The long-term spatial variation of *RE* or *Reref* is found to be mainly driven by the mean annual temperature [40–42], mean annual plant productivity [43,44], and mean annual moisture [45–47]. Thus, the functional description of *Reref* in this study is developed based on its dependencies on the temperature, productivity, and moisture factor (Figure 3). Since *Reref* becomes less suitable to capture site characteristics at higher *Tref* values [27], *Tref* was set as

the mean springtime (DOY 96-144) temperature (i.e., 3 °C for the Tibetan alpine grasslands, and 7 °C for the Inner Mongolian temperate grasslands), and the *Reref* for each site-year was calculated as the mean respiration rate at the temperature approximate to *Tref* during the spring time. Finally, *Reref* is estimated in our model as follows:

$$Reref = p_1 + p_2 * EVI_{mean} + p_3 * LST_{mean} + p_4 * LSWI_{mean},\qquad(4)$$

where EVI_{mean} is the mean annual springtime *EVI*, LST_{mean} is the mean annual daytime *LST* (LST_d), $LSWI_{mean}$ is the mean annual growing season *LSWI* (DOY 136-272), and p_1 to p_4 are parameters to be inferred herein. Figure 3 displays the *Reref* dependencies on EVI_{mean}, LST_{mean} and $LSWI_{mean}$.
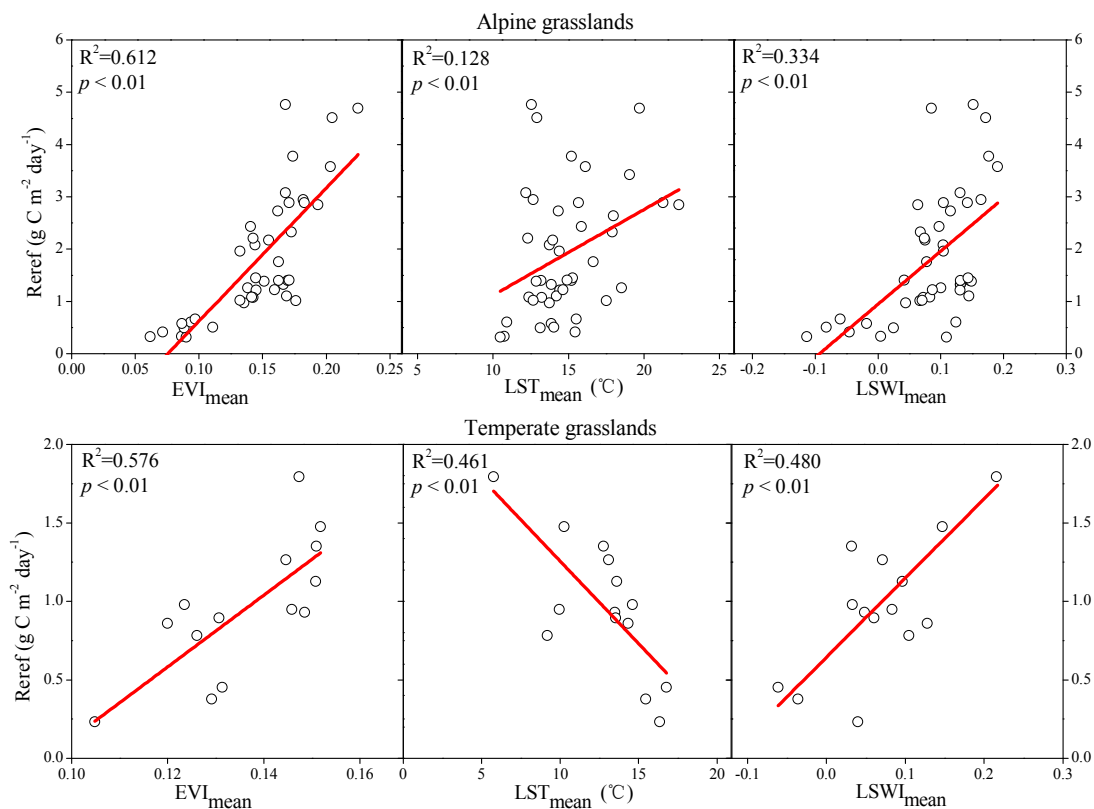

Figure 3. Reference respiration (*Reref*) response to the mean annual springtime *EVI* (EVI_{mean}), mean annual *LST* (LST_{mean}) and mean annual growing season *LSWI* ($LSWI_{mean}$) for the Tibetan alpine grasslands and the Inner Mongolian temperate grasslands.

2.3.2. Representation of Temporal Variability of *RE*

The seasonal dynamics of *RE* are reflected by $f(T,P,W)$, which is mainly controlled by the temporal variability of temperature [48,49], vegetation productivity [43,50], and water [20–22,40]. Especially in the arid and semi-arid ecosystems, water is the main limiting factor of the seasonality of *RE* [51,52]. The values of $f(T,P,W)$ are obtained by calculating the ratio of the observed *RE* from the flux tower and the site-specific *Reref* partitioned from the observed *RE*. Figure 4 displays the $f(T,P,W)$ dependencies on the temporal variation of *EVI*, *LST* and *LSWI*. The form of $f(LST,EVI)$ scalar was based on the *LST*-driven Lloyd-Taylor equation [48] and *EVI*-driven linear equation, while the form of f_W scalar was derived from a Michaelis-Menten equation firstly proposed by Raich et al. [53]. During the growing season, we calculate the $f(T,P,W)$ as follows:

$$f(T,P,W) = f(LST,EVI) * f_W,\qquad(5)$$

$$f(LST, EVI) = p_5 * \exp\left(E_0 * \left(\frac{1}{Tref - T_0} - \frac{1}{LST_n - T_0}\right)\right) + p_6 * EVI_{std} + p_7, \tag{6}$$

$$f_W = \frac{(0.5 + LSWI)}{k + (0.5 + LSWI)}, \tag{7}$$

where LST_n is nighttime *LST*, EVI_{std} is the standardized *EVI* (8-day *EVI* divided by EVI_{mean}), p_5 to p_7 are the parameters to be sought, E_0 is the activation energy, T_0 is the minimum temperature for respiration, which is set to 227.13 k (-46.02 °C) as in the original Lloyd-Taylor model, k is the half-saturation constant of the hyperbolic relationship, and 0.5 is an empirically given value to maintain the numerator/denominator of $fw > 0$.
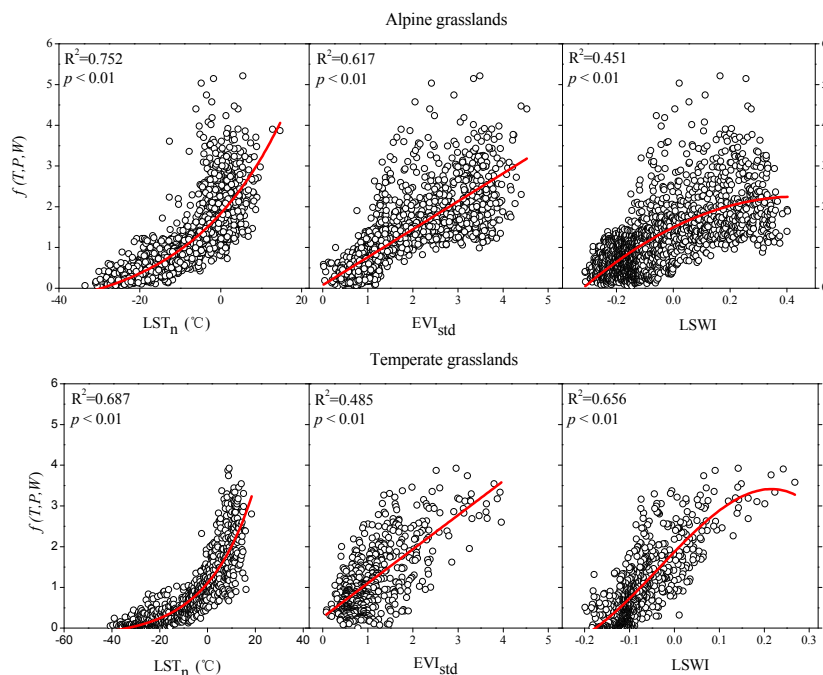

Figure 4. f (*T,P,W*) response to nighttime *LST* (LST_n), standardized *EVI* (EVI_{std}), and *LSWI* for the Tibetan alpine grasslands and the Inner Mongolian temperate grasslands.

During the non-growing season, temperature, but not water, becomes the main limiting factor for *RE* in northern China's grasslands [24]. In addition, the surface covered by ice and snow in the non-growing season has a strong absorption of the shortwave infrared band that causes *LSWI* to increase sharply; thus, it cannot reflect the actual water content in the winter [54]. Therefore, the *fw* scalar is only considered for the growing season (Equation (5)). During the non-growing season, we calculate the temporal variability of *RE* as follows:

$$f(T, P, W) = f(LST, EVI), \tag{8}$$

The different periods of MODIS indices (i.e., the mean springtime of *EVI*, the mean annual of LST_d in *Reref*, and LST_n in $f(T, P, W)$) used here have already been selected by Jägermeyr et al. [27] as the best index for fitting the relationship with RE. *LSWI*, selected by us as the model driver, is a more direct proxy for moisture than LST_{diff}, which was used in RECO but had no significant relation with the temporal dynamics of *RE* in our study ($R^2 < 0.2$, $p > 0.05$); in addition, land surface moisture was found to have greater influence on *RE* than deep soil water [20,28], which is especially instrumental in northern China's grasslands with the large number of roots distributed in the soil surface [55]. Therefore, all these drivers appear to be chosen empirically but are based on the physiological dependencies of *RE*, thereby ensuring reliable estimates from our model.

2.4. Model Parameterization and Validation

The two components, i.e. *Reref* for each site and year and the remaining seasonal variation *f(T,P,W)* partitioned from the overserved *RE*, were used to optimize parameters for Equations (4) and (5) separately to better constrain each component of the model. The nonlinear least-squares curve fitting method was utilized to estimate the model parameters. In addition to joint-sites estimation for the two grasslands in two regions, the leave-one-out cross validation method was employed to test the validity of the joint estimation of parameters (i.e., one subtype was excluded at a time, and the data for all other subtypes were used to estimate the parameters for each grassland type). The coefficient of determination (R^2) and root mean square error (RMSE) were chosen to assess the model performance. Regional-scale application is based on PFT-specific parameters retrieved from the entire site-data of alpine grasslands and temperate grasslands to assure most robust parameters.

To further verify the model improvement by incorporating the moisture effect on both spatial and temporal variability, the $LSWI_{mean}$ in *Reref* and *fw* in *f(T,P,W)* were removed, respectively, to test the accuracy of the model. In addition, we also compare some other semi-empirical or process-based models to assess the ability of our model. Specifically, for the *RE* estimation at a site scale, we chose the two original models that our model was based on, namely T&P [22] and RECO [27]; for the *RE* estimation at a regional scale, an independent regional *RE* product simulated by a mainstream dynamic global vegetation model CLM4CN, derived from Piao et al. [56], was applied.

3. Results

3.1. Quantitative Relationships between RE and Biotic and Climatic Factors

The observed *RE* values were partitioned into *Reref* and *f(T,P,W)* to account for the spatial and temporal variability of *RE* separately. The quantitative relationships between these two components and the climatic and biotic factors provided a clear physiological basis for the development of the model.

3.1.1. Quantitative Relationships between *Reref* and Biotic and Climatic Factors

Multiple regression analyses between *Reref* and the remote-sensing data show that *Reref* has a significant dependence on EVI_{mean}, LST_{mean} and $LSWI_{mean}$, which can be approximated linearly (Figure 3). The variation of *Reref* in the Tibetan alpine grasslands is primarily attributed to the change in vegetation productivity (EVI_{mean}, $R^2 = 0.612$) and to the water regime ($LSWI_{mean}$, $R^2 = 0.334$). Temperature plays a negligible role in the *Reref* (LST_{mean}, $R^2 = 0.128$). Similarly, productivity ($R^2 = 0.576$) and moisture ($R^2 = 0.480$) tend to be more important than temperature ($R^2 = 0.461$) for *Reref* in the temperate grasslands of Inner Mongolia. However, the temperature limitation among the temperate grassland sites is characterized by a negative slope.

3.1.2. Quantitative Relationships between $f(T, P, W)$ and Biotic and Climatic Factors

The regression analyses between $f(T, P, W)$ and the remote-sensing indexes (Figure 4) indicate that the temporal variability of *RE* has a strong exponential dependency on temperature, which could be described using the LST_n-driven Lloyd-Taylor equation. *RE* still has a significant linear response to the seasonal dynamics of *EVI*, which is decided by the behind mechanism that growth respiration supplies energy at the cost of consuming some photosynthate, causing the *RE* to be approximate to a constant fraction of plant productivity [57,58]. In terms of the response to temporal variation of *LSWI*, *RE* is almost linearly related to *LSWI* firstly (when *LSWI* < 0.1) and then it reaches saturation during the final stage in the Inner Mongolian region with a relatively low soil water content, whereas in the Tibetan region with a relatively high soil water content, the response of *RE* to *LSWI* follows a gradual saturation. The responses of *RE* to moisture under the two different water regimes both agree well with the typical Michaelis-Menten curve.

The temporal variation of *RE* in the alpine grasslands of the Tibetan Plateau is mainly correlated to temperature (LST_n, R^2 = 0.752), followed by plant productivity (EVI_{std}, R^2 = 0.617), while water (*LSWI*, R^2 = 0.451) plays a minor role in regulating the temporal dynamics of *RE* in this temperature-limited region (Figure 4). In contrast, water exerts a strong influence (*LSWI*, R^2 = 0.656) on the temporal variability of *RE* in the temperate grasslands of Inner Mongolia, which is comparable with the determinant factor (LST_n, R^2 = 0.687), while plant productivity exerts a relatively weak impact (EVI_{std}, R^2 = 0.485).

3.2. Model Parameterization and Validation

Based on the quantitative dependencies of spatiotemporal variability in *RE* to these biotic and environmental factors, we developed a semi-empirical *RE* model described in 2.3. The long-term flux tower-observed *RE* was used for parameter estimation and validation. Detailed parameter values for *Reref* and $f(T, P, W)$ in the two grasslands are presented in Table 2. These parameters are mostly empirical coefficients varying with the vegetation types and structures, site conditions, and histories. One of the parameters for *Reref*, for example, p_3, has the opposite sign for the temperate grasslands (negative) relative to the alpine grasslands (positive). This phenomenon implies a negative correlation between the spatial variation of *RE* and mean annual temperature in Inner Mongolia. Among the parameters for $f(T,P,W)$, the activation energy E_0 and the half saturation constant k are two key parameters that have a special physiological implication. In the alpine grasslands, E_0 has a higher value than the temperate grasslands. This result accurately reflects the increasing temperature sensitivity with the decreasing temperature. Regarding the half saturation constant, k, the value is higher (0.207) in the temperate grasslands than the alpine grasslands (0.021). The drier ecosystem has a higher half saturation point, accurately characterizing the different responses of *RE* to moisture among the alpine and the arid and semi-arid regions.

Table 2. Parameter estimation of *Reref* and $f(T,P,W)$ for two grassland types in two regions.

	Grassland Type	Alpine Grasslands		Temperate Grasslands	
Reref	p_1	-2.646 ± 0.456		-0.019 ± 0.023	
	p_2	15.100 ± 2.062		8.347 ± 1.068	
	p_3	0.173 ± 0.024		-0.029 ± 0.009	
	p_4	18.828 ± 0.939		3.952 ± 0.322	
$f(T,P,W)$	p_5	1.787 ± 0.081	(1.421 ± 0.136) *	0.658 ± 0.119	(0.941 ± 0.147) *
	E_0	279.764 ± 53.87	(164.507 ± 31.874) *	166.327 ± 12.402	(154.305 ± 18.729) *
	p_6	0.250 ± 0.024	(0.193 ± 0.046) *	0.944 ± 0.039	(0.085 ± 0.061) *
	p_7	0.094 ± 0.039	(0.108 ± 0.046) *	-0.363 ± 0.081	(0.190 ± 0.050) *
	k	0.021 ± 0.064		0.207 ± 0.0082	

* Among the parameters for $f(T,P,W)$, the values inside the parentheses are for the non-growing season, while the others are for the growing season.

The model parameter estimation reveals that approximately 77.8% and 74.9% of the variation in the observed *RE* across the alpine and temperate grasslands, respectively, could be explained by this model, albeit with a small bias (Figure 5; Table 3, joint-sites). Specifically, the model could explain more than 55% of the spatial variability of *RE* (*Reref*) in the two regions. The simulation error in the Tibetan alpine grasslands (RMSE = 0.62 g C m^{-2} day^{-1}) is higher than that in the Inner Mongolian temperate grasslands (RMSE = 0.11 g C m^{-2} day^{-1}). The temporal variability ($f(T,P,W)$) is generally explained to a greater degree (more than 65%) compared to the spatial variability, while the simulation error in the temperate grasslands (0.91 g C m^{-2} day^{-1}) is higher than that in the alpine grasslands (0.35 g C m^{-2} day^{-1}). The cross-validation among subtypes in the alpine and temperate grasslands shows that approximately 75.6–91.7% and 57.5–80.3%, respectively, of the variation in the observed *RE* could be predicted by the model, with the values of RMSE ranging from 0.841 to 1.544 g C m^{-2} day^{-1} and 0.405–1.021 g C m^{-2} day^{-1} for the alpine and temperate grasslands, respectively (Table 3). Except for the typical steppe, where the parameters derived from the limited sites in the meadow steppe and

desert steppe do not represent for the typical steppe well, the other vegetation types differ slightly in performances from the cross-validation and parameter estimation, which verifies the robustness of the parameterization results.
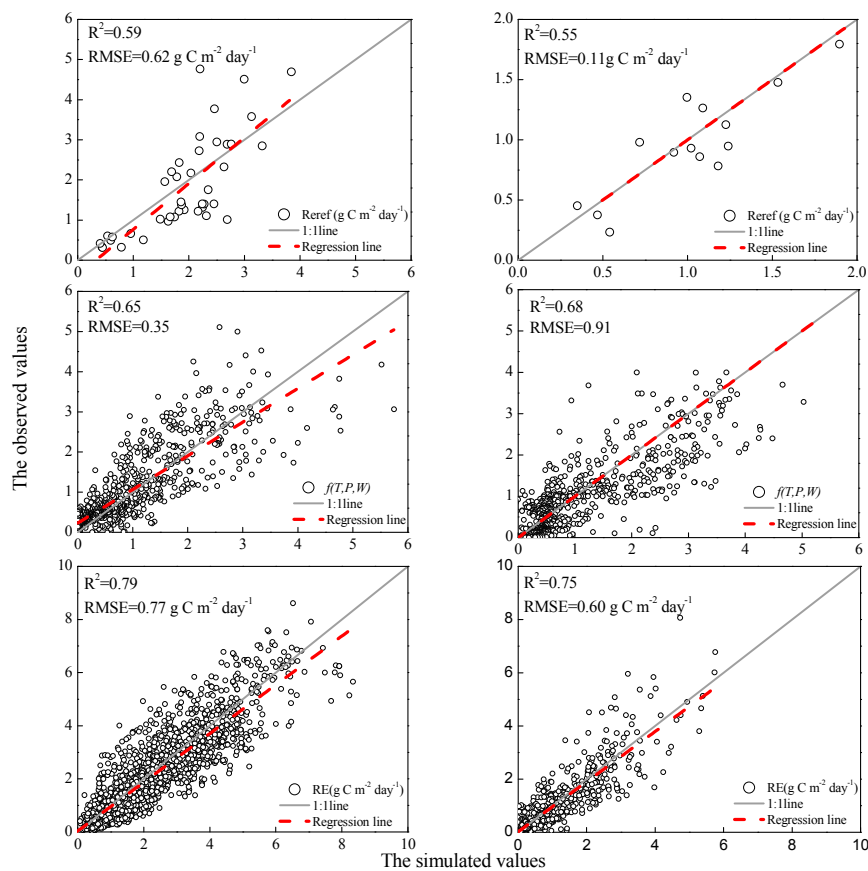

Figure 5. Comparison between the observed and predicted ecosystem respiration (*RE*) in the Tibetan alpine grasslands (**left**) and the Inner Mongolian temperate grasslands (**right**).

Table 3. Joint-sites estimation and leave-one-out cross validation for each vegetation type.

Vegetation Type	Types of Parameter Estimation	Types of Cross-Validation	R^2	RMSE	*p* Value
Alpine Grasslands	SH_SW_ST	KO	0.844	0.841	<0.01
	KO_SW_ST	SH	0.756	1.047	<0.01
	KO_SH_ST	SW	0.917	0.927	<0.01
	KO_SH_SW	ST	0.784	1.544	<0.01
	Joint-sites (AR_GL_HBKO_GL)	/	0.778	0.774	<0.01
Temperate Grasslands	TS_DS	MS	0.803	0.405	<0.01
	MS_DS	TS	0.575	0.919	<0.01
	TS_MS	DS	0.643	1.021	<0.01
	Joint-sites (TS_MS_DS)	/	0.749	0.605	<0.01

3.3. Model Simulation for Seasonal and Inter-Annual Dynamics of RE at the Site Scale

Using the model parameters in Table 2, we simulate time-series *RE* of all 57 site-years and then further compared them to the flux tower-observed *RE* for each vegetation subtype in the alpine and temperate grasslands. In most cases, the temporal variation of the *RE* is tracked robustly by our model (Figure 6). The agreement between the modeled and observed *RE* is the best for the desert steppe and meadow steppe ($R^2 > 0.9$), followed by the alpine shrub meadow ($R^2 = 0.872$), the alpine meadow steppe ($R^2 = 0.805$), the alpine *Kobresia* meadow ($R^2 = 0.778$), the typical steppe ($R^2 = 0.743$), and the alpine swamp meadow ($R^2 = 0.715$). Ground covered by water in the alpine swamp meadow would

affect the spectral reflectance and further disturb the model drivers (*EVI* and *LSWI*), and this may be the main reason for the relatively low performance in this vegetation type.
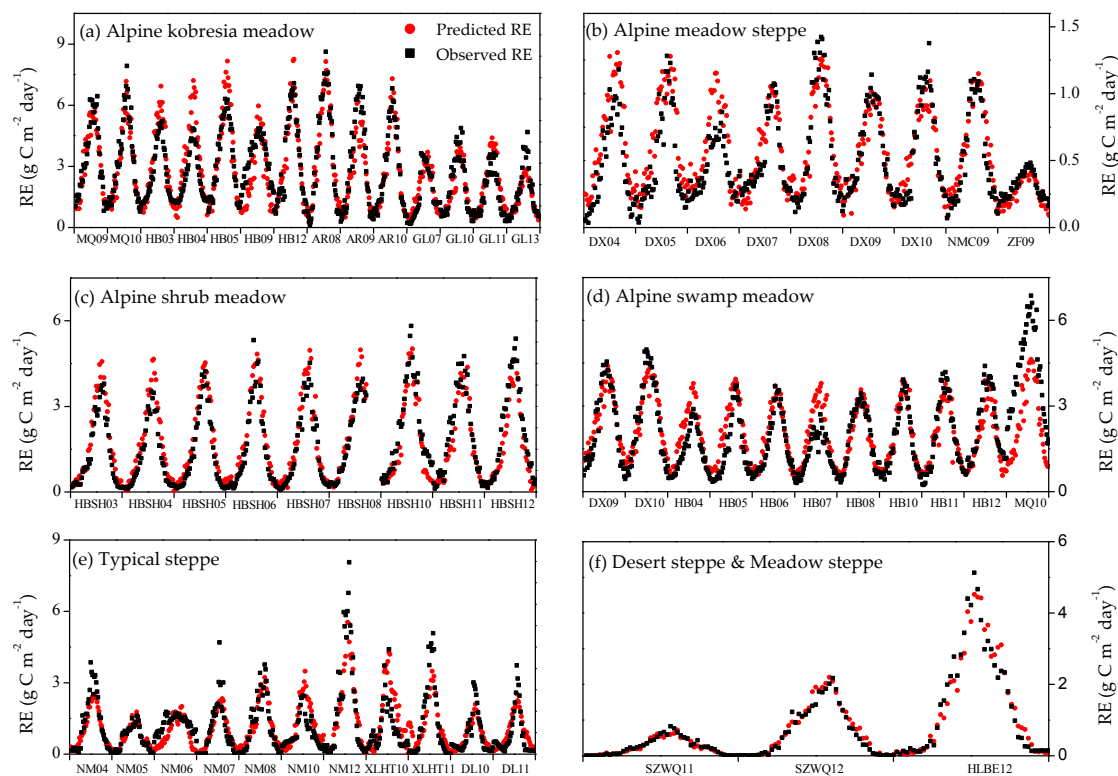

Figure 6. Time-series plots for observed (black square dot) and modeled (red round dot) ecosystem respiration (*RE*) at all sites. The text in the abscissa represents the abbreviation of the site name, and the following number represents the year.

The seasonal variation of *RE* in China's grasslands could be described as a unimodal curve peaking in July or August. Across the seven vegetation types, the mean annual peak respiration rate ranges from 1.10 to 5.84 g C m^{-2} day^{-1}. The highest value occurring in the alpine meadow or the meadow steppe is approximately four times higher than that of the alpine meadow steppe or the desert steppe. There are also significant inter-annual fluctuations in the *RE* at some sites; for instance, the observed *RE* decreased remarkably as precipitation decreased in 2011 in SZWQ (Figure 6f), 2005 and 2006 in NM (Figure 6e), and 2009 in HBKO (Figure 6a). In addition, our model could accurately reproduce the inter-annual dynamics of *RE* due to the variation in precipitation across years.

3.4. Model Simulation for Spatial Patterns of RE at the Regional Scale

Based on the parametrized *RE* model dependent on prescribed PFTs (alpine and temperate grasslands in Figure 1) and the spatial driver data of MODIS *EVI*, *LST*, and *LSWI*, the spatial distribution of the mean annual REs from 2001 to 2010 were obtained (Figure 7a). The predicted annual *RE* of China's northern grasslands is 258.18 $\pm$ 12.07 g C m^{-2} yr^{-1} on average. For the alpine grasslands on the Tibetan Plateau, the alpine shrub meadow has the largest *RE* value (434.69 $\pm$ 8.83 g C m^{-2} yr^{-1}), followed by the alpine swamp meadow (413.82 $\pm$ 8.21 g C m^{-2} yr^{-1}), the alpine *Kobresia* meadow (368.64 $\pm$ 7.52 g C m^{-2} yr^{-1}), and the alpine steppe meadow (146.57 $\pm$ 3.21 g C m^{-2} yr^{-1}), exhibiting a clear decreasing gradient from the southeast to the northwest with increasing elevation across the Tibetan Plateau. For the Inner Mongolian Plateau, *RE* also shows a clear decreasing gradient from northeast to southwest. Specifically, the highest value of *RE* occurs in the meadow steppe (470.27 $\pm$ 39.24 g C m^{-2} yr^{-1}) in the northeast, and the lowest value of *RE* occurs in the desert

steppe in the southwest (144.91 ± 21.75 g C m^{-2} yr^{-1}). The mean annual *RE* in the typical steppe is 193.6 ± 30.84 g C m^{-2} yr^{-1}.
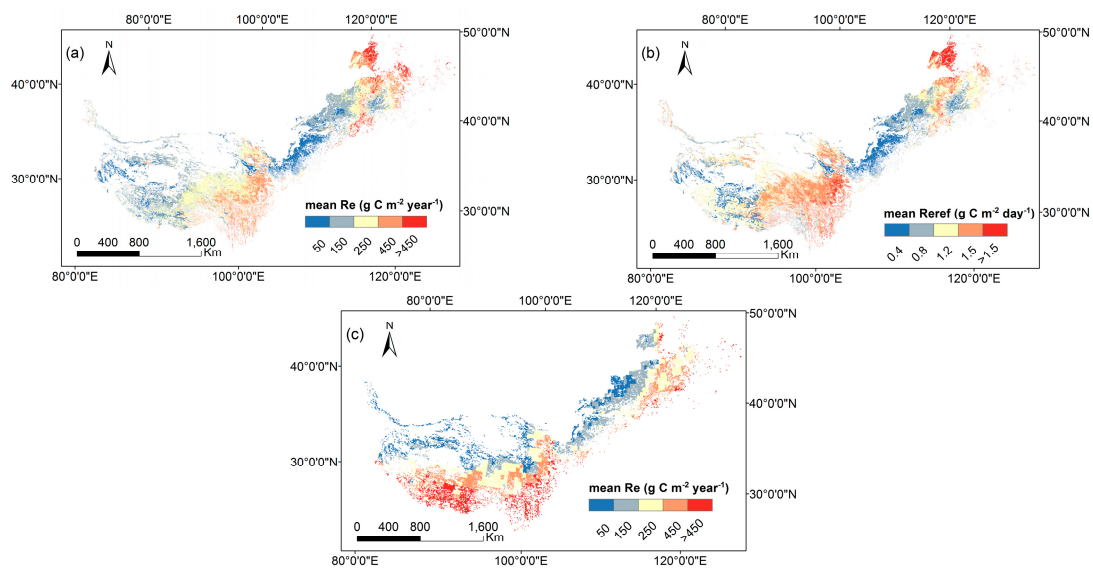

Figure 7. Predicted spatial distribution of the mean annual ecosystem respiration (RE). (**a**) and the reference respiration (*Reref*); (**b**) by our model and mean annual *RE* by CLM4CN; (**c**) in northern China's grasslands.

Reref appears to be a key component in this model in terms of quantifying the spatial variability of *RE* across sites. Nevertheless, the spatial patterns of *Reref* have rarely been investigated due to the lack of spatially explicit algorithms to allow the upscaling of *Reref*. Here, we took abiotic and biotic factors into consideration to parameterize *Reref* spatially and revealed that the mean annual *Reref* has a clear spatial heterogeneity among different vegetation types in northern China's grasslands (Figure 7b), ranging from 0.22 g C m^{-2} day^{-1} in the desert steppe to 2.25 g C m^{-2} day^{-1} in the meadow steppe. In addition, the spatial distribution of *Reref*, to a large extent, determines the spatial pattern of the mean annul *RE* (Figure 7a,b).

4. Discussion

4.1. Biotic and Climatic Control over RE

Our analysis reveals that among biotic and climatic factors, plant productivity and moisture exert stronger influences than temperature on regulating the spatial pattern of *RE*. These two factors together can well explain the spatial patterns of *RE*, accounting for 54% and 58% of the variation in the temperate grasslands and alpine grasslands, respectively (Table 4). The important role of plant productivity and moisture in regulating the spatial pattern of *RE* is in good accordance with other studies across the world [20,46,59,60]. Most of the variation in *RE* could be attributed to the difference in plant productivity among sites, with a relatively smaller proportion being further explained by moisture, but the moisture effect differs significantly between the two grasslands and plays a more crucial role in the water-deficit temperate grasslands than the alpine grasslands (Figure 3, Table 4).

Table 4. Relationship between *Reref* and the combined effects of EVI_{mean}, LST_{mean}, and $LSWI_{mean}$.

Grassland Type	EVI_{mean}		EVI_{mean} & $LSWI_{mean}$		EVI_{mean} & $LSWI_{mean}$ & LST_{mean}	
	R^2	RMSE (g C m^{-2} day^{-1})	R^2	RMSE (g C m^{-2} day^{-1})	R^2	RMSE (g C m^{-2} day^{-1})
Temperate grasslands	0.424	0.147	0.541	0.125	0.554	0.113
Alpine grasslands	0.539	0.714	0.577	0.653	0.588	0.617

Although temperature has been noted to be positively correlated with *RE* across biomes at a global scale [40,41] and an important limitation on *RE* in alpine ecosystems, the inclusion of LST_{mean} does not significantly affect the explanation of *Reref* variation (Table 4). In the alpine grasslands, studies increasingly suggest that plant biomass is the direct determinant of *RE* distribution [61–63], while moisture changes, but not temperature, serve as another indirect determinant via regulating plant growth and distribution in the vast alpine grasslands (4400–4800 m) [64]. The above two explanations describe how temperature is less important to governing the spatial pattern of *RE* in the alpine grasslands. However, the dependence of *Reref* on LST_{mean} appears to be stronger and negative in the temperate grasslands (Figure 3, Table 2). In fact, the relation of *RE* with temperature can be confounded by moisture in arid and semi-arid ecosystems [63,65]. Specifically, the gradient of precipitation mainly defines the declining gradient of *RE* from the northeast to the southwest in the Inner Mongolian Plateau, which is exactly opposite to the gradient of temperature [66], thus leading to the apparently close and negative spatial correlation between temperature and *RE*.

In contrast, temperature becomes the major controlling factor in terms of the temporal pattern of *RE* (Figure 4). The significant exponential dependence of seasonal *RE* on temperature that was observed in these two regions is consistent with many other grassland ecosystems [67,68]. However, there are obvious differences in the temperature control over *RE* among different climate zones. For the alpine grasslands, temperature explained 75.2% of the seasonal variability of *RE* and was the strongest controlling factor. However, the magnitude of the temporal dynamics of *RE* due to temperature decreased to 68.7% for the temperate grasslands. This result is in accordance with the argument that the seasonal variation of *RE* may depend much less on temperature when moisture become a limiting factor [23,65,69]. As expected, moisture exerts a strong impact on the seasonal changes of *RE* in the arid and semi-arid temperate grasslands, almost to the same degree as temperature (Figure 4). While the dependence of *RE* on *LSWI* is relatively weak, productivity serves as a relatively stronger controlling factor (Figure 4). Although some studies support the close correlation between the seasonal dynamics of *RE* and plant growth [68,70], this correlation still contradicts the more universal argument that the abiotic factors (temperature and moisture), rather than biotic factors (plant growth), mainly regulate the seasonal patterns of *RE* [67]. The most significant cause of this strong dependency on production in alpine grasslands is the relatively high root biomass density in this grassland community [71]; thus, autotrophic respiration, which is closely related to plant biomass, contributes to a relatively large proportion of the total *RE* [62].

4.2. Model Evaluation

The model demonstrates that flux-tower observed *RE* can be estimated with an applicable degree of accuracy across grasslands using only remote sensing data. We first evaluate the precision of our model at a site scale by comparing it to other recent semi-empirical approaches, e.g., the two original developed-based models, T&P [22] and RECO [27] that achieved a mean site-level accuracy of $R^2 = 0.679$ with RMSE =1.227 g C m^{-2} day^{-1} and $R^2 = 0.625$ with RMSE = 0.969 g C m^{-2} day^{-1}, respectively, for these 16 grassland sites, while our model performed better with a higher degree of explanation and a lower bias (Table 3), verifying the model improvements with better representation of *Reref* and further incorporation of the moisture effect. An independent regional *RE* product from a popular process-based model CLM4CN [56] was employed to further evaluate the model performance at a regional scale. The CLM4CN presented a mean annual *RE* value (309.18 ± 5.15) within an order of magnitude of this study, but it still resulted in an overestimation. The general spatial pattern of *RE* appeared similar but there were still distinct differences, especially in the water-deficit area. For example, in the southwest of the desert grasslands which is driest, the CLM4CN failed to produce the lowest values. Moreover, the CLM4CN unreasonably produced a higher *RE* in the alpine meadow steppe than the surrounding alpine meadow (Figure 7a,c). These distinct differences are likely associated with the different representation of *Reref* in the models, which has been proven to largely determine the spatial pattern of *RE* (Figure 7a,b). *Reref* was set as the same constant for all

biomes in the CLM4CN [72], as in the most process-based models [73–75]. However, more and more studies demonstrate that a large error would be introduced if a constant *Reref* is used [76]. In fact, *Reref* varies remarkably in space [9,22,60]. Therefore, the better representation of *Reref* makes our model more sensible for capturing the regional characteristics of *RE* in grassland ecosystems and arid and semi-arid areas, in particular.

The consideration of moisture effects on both the spatial and temporal variabilities of *RE* is another major factor contributing to the better performance of our model. For the spatial variability of *RE* (*Reref*), even though it has been gradually confirmed to vary systematically with the spatial variation of productivity (GPP or LAI) and temperature [8,20–22,27,50], to our knowledge, this process has not yet been linked to moisture change in satellite-based *RE* studies at large scales and with a high resolution. Our findings reveal that *Reref* has a significant linear relation with $LSWI_{mean}$ in both the Tibetan and Inner Mongolian grasslands (Figure 3, $p < 0.01$), which is also supported by another recent study in northern China [24]. Considerable improvement was found in the explanation of *Reref* (12%, Table 4) in the temperate grasslands by the inclusion of the moisture effect, while the improvement is relatively small (4%) in the alpine grasslands due to the colinearity of plant biomass and soil moisture [62].

Moisture also exerts significant influence on the seasonal dynamics of *RE* in northern China's grasslands (Figure 4), which further explained a large proportion of *RE* in the arid and semi-arid vegetation types (Table 5). Obvious gaps would be found in the performance between the model without *fw* and the model with *fw* for the arid and semi-arid ecosystems. The simulated *RE* with *fw* has a higher correlation coefficient with observed values (R^2 increased by 12–24%) and a smaller bias from the observed values (RMSE reduced by 13–41%) in the desert steppe, typical steppe, and alpine meadow steppe. Although various equations (e.g., linear, quadratic, parabolic, logarithmic, exponential, and hyperbolic form) have been proposed to describe the response process of *RE* to moisture [69,77,78], our findings reveal that the Michaelis-Menten equation is the most applicable form for northern China's grasslands, as the moisture content is hardly able to reach beyond field capacity and toward saturation in these water-limited grasslands [62,66]. Therefore, the process of the steep decline in *RE* at very high moisture levels could be ignored, while the remaining two phases, i.e., the strong increase at low moisture levels and the plateau of *RE* in response to a broad range of near optimum water contents, agree well with the typical Michaelis-Menten-shaped curve.

Table 5. Comparison of model performance between the model without *fw* and the model with *fw* for each vegetation type.

Vegetation Type	Model without *fw*		Model with *fw*	
	R^2	RMSE (g C m^{-2} day^{-1})	R^2	RMSE (g C m^{-2} day^{-1})
Typical steppe	0.68	0.70	0.74	0.61
Desert steppe	0.78	0.22	0.97	0.13
Meadow steppe	0.94	0.35	0.95	0.34
Alpine *Kobresia* meadow	0.75	1.09	0.78	0.93
Alpine meadow steppe	0.71	0.21	0.81	0.16
Alpine swamp meadow	0.69	0.77	0.72	0.74
Alpine shrub meadow	0.86	0.74	0.88	0.72

4.3. Model Applications and Limitations

Our model was developed with a robust biological basis with long-term and inter-sites observations, and it performed well in estimating *RE* for northern China's grasslands solely driven by MODIS products. The main advances introduced by this model are the better representation of the *Reref* process and the comprehensive consideration of moisture effect combined with temperature and productivity effects on *RE*. The derived parameters reported in Table 2 may be considered as an optimized parameterization for the application of the model at a regional scale. Our model may facilitate the simulation of *RE* at larger spatial scales with a high temporal resolution and could also

be combined with the satellite-based GPP models or MODIS-retrieved GPP products to conduct a regional-scale NEE simulation.

However, the further application of our model at a larger scale probably has several limitations: (1) The spatial variability (*Reref*) is explained to a relatively lower degree compared to the temporal variability (*f*(*T*,*W*,*P*)). Since *RE* is also influenced by a number of other biotic and abiotic factors, such as age of the ecosystem [57], nutrient availability [79], and acclimation and disturbance effects, we expect that more comprehensive information could be incorporated in the model to better represent the variations of *Reref*; (2) Although the satellite-derived VIs can to some extent reflect the impacts of GPP on respiration [80,81] and have also been widely used to explain the seasonal variation in Rs as VIs are related to soil carbon through litter input [16,82,83], they are still difficult to mirror in terms of the influence of the belowground organic matter on *RE*; (3) The performance of our model for other vegetation types or in other regions needs to be validated in further study. Without further testing, the model is strictly applicable to similar ecosystems (i.e., temperate and alpine grassland ecosystems). Along with the development of satellite algorithms for soil moisture, plant biomass, nutrient availability, human activity, and so on, we will optimize the model to improve its accuracy.

5. Conclusions and Implications

A statistical-mechanistic model driven by remote-sensing data was formulated for simulating the spatial and temporal variability of *RE*. The effect of plant productivity, temperature, and moisture were comprehensively considered using the publicly available MODIS products *EVI*, *LST*, and *LSWI*, thereby yielding a better performance for the *RE* simulation across seven vegetation types in the Tibetan alpine grasslands and Inner Mongolian temperate grasslands. The temporal variations as well as the spatial patterns of *RE* in northern China's grasslands were well reproduced by the model. The inclusion of *LSWI* in the *Reref* and the seasonal dynamics of *RE* significantly improved the model performance in arid and semi-arid ecosystems. Our results suggest that a good representation of the spatial process and moisture effect on *RE* should be considered in the next-generation satellite-based *RE* models.

Biotic and climatic control over *RE* is different for temporal and spatial processes. Plant productivity and moisture mainly contribute to the spatial variation of *RE* in northern China's grasslands. The influence of moisture on the spatial pattern of *RE* is stronger in the temperate grasslands than in the alpine grasslands. Temperature plays a minor role in regulating the spatial pattern of *RE*. In contrast, temperature tends to be more important in controlling the seasonal patterns of *RE* in northern China's grasslands, whereas in the temperate grasslands of Inner Mongolia, moisture exerts strong impact on the seasonal variation of *RE*, almost equally important as temperature. These conclusions drawn from the Tibetan and Inner Mongolian grasslands, on behalf of the alpine grasslands and Eurasian temperate grasslands across the word, can provide valuable information for large–scale estimates of *RE* and better understanding the response of *RE* to climate change in grassland ecosystems.

References

1. Adams, J.M.; Faure, H.; Faure-Denard, L.; McGlade, J.; Woodward, F. Increases in terrestrial carbon storage from the last glacial maximum to the present. *Nature* **1990**, *348*, 711–714. [CrossRef]

2. World Resources Institute. Taking stock of ecosystems-grassland ecosystems. In *World Resources 2000–2001: People and Ecosystems—The Fraying Web of Life*; World Resources Institute: Washington, DC, USA, 2000; pp. 119–131.

3. Ni, J. Carbon storage in grasslands of china. *J. Arid Environ.* **2002**, *50*, 205–218. [CrossRef]

4. Kang, L.; Han, X.; Zhang, Z.; Sun, O.J. Grassland ecosystems in china: Review of current knowledge and research advancement. *Philos. Trans. R. Soc. B* **2007**, *362*, 997–1008. [CrossRef] [PubMed]

5. Ma, W.; Fang, J.; Yang, Y.; Mohammat, A. Biomass carbon stocks and their changes in Northern China's grasslands during 1982–2006. *Sci. China Life Sci.* **2010**, *53*, 841–850. [CrossRef] [PubMed]

6. Guo, Q.; Hu, Z.; Li, S.; Li, X.; Sun, X.; Yu, G. Spatial variations in aboveground net primary productivity along a climate gradient in Eurasian temperate grassland: Effects of mean annual precipitation and its seasonal distribution. *Glob. Chang. Biol.* **2012**, *18*, 3624–3631. [CrossRef]

7. Chen, H.; Zhu, Q.; Peng, C.; Wu, N.; Wang, Y.; Fang, X.; Gao, Y.; Zhu, D.; Yang, G.; Tian, J. The impacts of climate change and human activities on biogeochemical cycles on the Qinghai-Tibetan Plateau. *Glob. Chang. Biol.* **2013**, *19*, 2940–2955. [CrossRef] [PubMed]

8. Yuan, W.; Luo, Y.; Li, X.; Liu, S.; Yu, G.; Zhou, T.; Bahn, M.; Black, A.; Desai, A.R.; Cescatti, A. Redefinition and global estimation of basal ecosystem respiration rate. *Glob. Biogeochem. Cycle* **2011**, *25*. [CrossRef]

9. Davidson, E.A.; Janssens, I.A.; Luo, Y. On the variability of respiration in terrestrial ecosystems: Moving beyond q10. *Glob. Chang. Biol.* **2006**, *12*, 154–164. [CrossRef]

10. Anav, A.; Friedlingstein, P.; Kidston, M.; Bopp, L.; Ciais, P.; Cox, P.; Jones, C.; Jung, M.; Myneni, R.; Zhu, Z. Evaluating the land and ocean components of the global carbon cycle in the cmip5 earth system models. *J. Clim.* **2013**, *26*, 6801–6843. [CrossRef]

11. Olofsson, P.; Lagergren, F.; Lindroth, A.; Lindström, J.; Klemedtsson, L.; Eklundh, L. Towards operational remote sensing of forest carbon balance across Northern Europe. *Biogeoscience* **2007**, *4*, 3143–3193. [CrossRef]

12. Yamaji, T.; Sakai, T.; Endo, T.; Baruah, P.J.; Akiyama, T.; Saigusa, N.; Nakai, Y.; Kitamura, K.; Ishizuka, M.; Yasuoka, Y. Scaling-up technique for net ecosystem productivity of deciduous broadleaved forests in japan using Modis data. *Ecol. Res.* **2008**, *23*, 765–775. [CrossRef]

13. Schubert, P.; Eklundh, L.; Lund, M.; Nilsson, M. Estimating northern peatland CO_2 exchange from Modis time series data. *Remote Sens. Environ.* **2010**, *114*, 1178–1189. [CrossRef]

14. Gilmanov, T.G.; Tieszen, L.L.; Wylie, B.K.; Flanagan, L.B.; Frank, A.B.; Haferkamp, M.R.; Meyers, T.P.; Morgan, J.A. Integration of CO_2 flux and remotely-sensed data for primary production and ecosystem respiration analyses in the northern great plains: Potential for quantitative spatial extrapolation. *Glob. Ecol. Biogeogr.* **2005**, *14*, 271–292. [CrossRef]

15. Loranty, M.M.; Goetz, S.J.; Rastetter, E.B.; Rocha, A.V.; Shaver, G.R.; Humphreys, E.R.; Lafleur, P.M. Scaling an instantaneous model of tundra nee to the arctic landscape. *Ecosystems* **2011**, *14*, 76–93. [CrossRef]

16. Huang, N.; He, J.-S.; Niu, Z. Estimating the spatial pattern of soil respiration in Tibetan alpine grasslands using landsat tm images and Modis data. *Ecol. Indic.* **2013**, *26*, 117–125. [CrossRef]

17. Rahman, A.; Sims, D.; Cordova, V.; El-Masri, B. Potential of Modis Evi and surface temperature for directly estimating per-pixel ecosystem C fluxes. *Geophys. Res. Lett.* **2005**, *32*. [CrossRef]

18. Sims, D.A.; Rahman, A.F.; Cordova, V.D.; El-Masri, B.Z.; Baldocchi, D.D.; Bolstad, P.V.; Flanagan, L.B.; Goldstein, A.H.; Hollinger, D.Y.; Misson, L. A new model of gross primary productivity for North American ecosystems based solely on the enhanced vegetation index and land surface temperature from Modis. *Remote Sens. Environ.* **2008**, *112*, 1633–1646. [CrossRef]

19. Wu, C.; Gaumont-Guay, D.; Black, T.A.; Jassal, R.S.; Xu, S.; Chen, J.M.; Gonsamo, A. Soil respiration mapped by exclusively use of Modis data for forest landscapes of Saskatchewan, Canada. *ISPRS J. Photogramm.* **2014**, *94*, 80–90. [CrossRef]

20. Reichstein, M.; Rey, A.; Freibauer, A.; Tenhunen, J.; Valentini, R.; Banza, J.; Casals, P.; Cheng, Y.; Grünzweig, J.M.; Irvine, J. Modeling temporal and large-scale spatial variability of soil respiration from soil water availability, temperature and vegetation productivity indices. *Glob. Biogeochem. Cycle* **2003**, *17*. [CrossRef]

21. Reichstein, M.; Ciais, P.; Papale, D.; Valentini, R.; Running, S.; Viovy, N.; Cramer, W.; Granier, A.; Ogee, J.; Allard, V. Reduction of ecosystem productivity and respiration during the European summer 2003 climate anomaly: A joint flux tower, remote sensing and modelling analysis. *Glob. Chang. Biol.* **2007**, *13*, 634–651. [CrossRef]

22. Migliavacca, M.; Reichstein, M.; Richardson, A.D.; Colombo, R.; Sutton, M.A.; Lasslop, G.; Tomelleri, E.; Wohlfahrt, G.; Carvalhais, N.; Cescatti, A. Semiempirical modeling of abiotic and biotic factors controlling ecosystem respiration across eddy covariance sites. *Glob. Chang. Biol.* **2011**, *17*, 390–409. [CrossRef]

23. Wohlfahrt, G.; Anderson-Dunn, M.; Bahn, M.; Balzarolo, M.; Berninger, F.; Campbell, C.; Carrara, A.; Cescatti, A.; Christensen, T.; Dore, S. Biotic, abiotic, and management controls on the net ecosystem CO_2 exchange of European mountain grassland ecosystems. *Ecosystems* **2008**, *11*, 1338–1351. [CrossRef]

24. Gao, Y.; Yu, G.; Li, S.; Yan, H.; Zhu, X.; Wang, Q.; Shi, P.; Zhao, L.; Li, Y.; Zhang, F. A remote sensing model to estimate ecosystem respiration in northern china and the Tibetan plateau. *Ecol. Model.* **2015**, *304*, 34–43. [CrossRef]

25. Knapp, A.K.; Smith, M.D. Variation among biomes in temporal dynamics of aboveground primary production. *Science* **2001**, *291*, 481–484. [CrossRef] [PubMed]

26. Fu, Y.L. Environmental Controls on Carbon Budgets in Typical Grassland Ecosystems on Chinese Grassland Transect. Ph.D. Thesis, Institute of Geographic Sciences and Natural Resources Research, Chinese Academy of Sciences, Beijing, China, 2006.

27. Jägermeyr, J.; Gerten, D.; Lucht, W.; Hostert, P.; Migliavacca, M.; Nemani, R. A high-resolution approach to estimating ecosystem respiration at continental scales using operational satellite data. *Glob. Chang. Biol.* **2014**, *20*, 1191–1210. [CrossRef] [PubMed]

28. Huang, N.; Gu, L.; Niu, Z. Estimating soil respiration using spatial data products: A case study in a deciduous broadleaf forest in the Midwest USA. *J. Geophys. Res. Atmos.* **2014**, *119*, 6393–6408. [CrossRef]

29. Atkin, O.K.; Bloomfield, K.J.; Reich, P.B.; Tjoelker, M.G.; Asner, G.P.; Bonal, D.; Bönisch, G.; Bradford, M.G.; Cernusak, L.A.; Cosio, E.G. Global variability in leaf respiration in relation to climate, plant functional types and leaf traits. *New Phytol.* **2015**, *206*, 614–636. [CrossRef] [PubMed]

30. Doughty, C.E.; Metcalfe, D.; Girardin, C.; Amézquita, F.F.; Cabrera, D.G.; Huasco, W.H.; Silva-Espejo, J.; Araujo-Murakami, A.; Da Costa, M.; Rocha, W. Drought impact on forest carbon dynamics and fluxes in Amazonia. *Nature* **2015**, *519*, 78–82. [CrossRef] [PubMed]

31. Church, J.; Clark, P.; Cazenave, A.; Gregory, J.; Jevrejeva, S.; Levermann, A.; Merrifield, M.; Milne, G.; Nerem, R.; Nunn, P. Contribution of working group i to the fifth assessment report of the intergovernmental panel on climate change. *Clim. Chang.* **2013**, 1138–1191.

32. Zhang, J.-W. *Vegetation of Xizang (Tibet)*; Science Press: Beijing, China, 1988.

33. Bai, Y.; Wu, J.; Xing, Q.; Pan, Q.; Huang, J.; Yang, D.; Han, X. Primary production and rain use efficiency across a precipitation gradient on the Mongolia plateau. *Ecology* **2008**, *89*, 2140–2153. [CrossRef] [PubMed]

34. Yu, G.-R.; Wen, X.-F.; Sun, X.-M.; Tanner, B.D.; Lee, X.; Chen, J.-Y. Overview of Chinaflux and evaluation of its eddy covariance measurement. *Agric. For. Meteorol.* **2006**, *137*, 125–137. [CrossRef]

35. Reichstein, M.; Falge, E.; Baldocchi, D.; Papale, D.; Aubinet, M.; Berbigier, P.; Bernhofer, C.; Buchmann, N.; Gilmanov, T.; Granier, A. On the separation of net ecosystem exchange into assimilation and ecosystem respiration: Review and improved algorithm. *Glob. Chang. Biol.* **2005**, *11*, 1424–1439. [CrossRef]

36. Li, C.; He, H.; Liu, M.; Su, W.; Fu, Y.; Zhang, L.; Wen, X.; Yu, G. The design and application of CO_2 flux data processing system at Chinaflux. *Geo-Inf. Sci.* **2008**, *10*, 557–565.

37. Huete, A.; Didan, K.; Miura, T.; Rodriguez, E.P.; Gao, X.; Ferreira, L.G. Overview of the radiometric and biophysical performance of the Modis vegetation indices. *Remote Sens. Environ.* **2002**, *83*, 195–213. [CrossRef]

38. Jönsson, P.; Eklundh, L. Timesat—A program for analyzing time-series of satellite sensor data. *Comput. Geosci.-UK* **2004**, *30*, 833–845. [CrossRef]

39. Reichstein, M.; Beer, C. Soil respiration across scales: The importance of a model–data integration framework for data interpretation. *J. Plant Nutr. Soil Sci.* **2008**, *171*, 344–354. [CrossRef]

40. Raich, J.W.; Schlesinger, W.H. The global carbon dioxide flux in soil respiration and its relationship to vegetation and climate. *Tellus B* **1992**, *44*, 81–99. [CrossRef]

41. Raich, J.W.; Potter, C.S. Global patterns of carbon dioxide emissions from soils. *Glob. Biogeochem. Cycle* **1995**, *9*, 23–36. [CrossRef]

42. Chen, Z.; Yu, G.; Ge, J.; Wang, Q.; Zhu, X.; Xu, Z. Roles of climate, vegetation and soil in regulating the spatial variations in ecosystem carbon dioxide fluxes in the northern hemisphere. *PLoS ONE* **2015**, *10*, e0125265. [CrossRef] [PubMed]

43. Janssens, I.; Lankreijer, H.; Matteucci, G.; Kowalski, A.; Buchmann, N.; Epron, D.; Pilegaard, K.; Kutsch, W.; Longdoz, B.; Grünwald, T. Productivity overshadows temperature in determining soil and ecosystem respiration across European forests. *Glob. Chang. Biol.* **2001**, *7*, 269–278. [CrossRef]

44. Sampson, D.; Janssens, I.; Curiel Yuste, J.; Ceulemans, R. Basal rates of soil respiration are correlated with photosynthesis in a mixed temperate forest. *Glob. Chang. Biol.* **2007**, *13*, 2008–2017. [CrossRef]

45. Epstein, H.E.; Burke, I.C.; Lauenroth, W.K. Regional patterns of decomposition and primary production rates in the US great plains. *Ecology* **2002**, *83*, 320–327.

46. McCulley, R.L.; Burke, I.C.; Nelson, J.A.; Lauenroth, W.K.; Knapp, A.K.; Kelly, E.F. Regional patterns in carbon cycling across the great plains of North America. *Ecosystems* **2005**, *8*, 106–121. [CrossRef]

47. Noormets, A.; Desai, A.; Cook, B.; Euskirchen, E.; Ricciuto, D.; Davis, K.; Bolstad, P.; Schmid, H.; Vogel, C.; Carey, E. Moisture sensitivity of ecosystem respiration: Comparison of 14 forest ecosystems in the upper great lakes region, USA. *Agric. For. Meteorol.* **2008**, *148*, 216–230. [CrossRef]

48. Lloyd, J.; Taylor, J. On the temperature dependence of soil respiration. *Funct. Ecol.* **1994**, *8*, 315–323. [CrossRef]

49. Raich, J.W.; Tufekciogul, A. Vegetation and soil respiration: Correlations and controls. *Biogeochemistry* **2000**, *48*, 71–90. [CrossRef]

50. Migliavacca, M.; Reichstein, M.; Richardson, A.D.; Mahecha, M.D.; Cremonese, E.; Delpierre, N.; Galvagno, M.; Law, B.E.; Wohlfahrt, G.; Andrew Black, T. Influence of physiological phenology on the seasonal pattern of ecosystem respiration in deciduous forests. *Glob. Chang. Biol.* **2015**, *21*, 363–376. [CrossRef] [PubMed]

51. Davidson, E.A.; Verchot, L.V.; Cattanio, J.H.; Ackerman, I.L.; Carvalho, J. Effects of soil water content on soil respiration in forests and cattle pastures of eastern Amazonia. *Biogeochemistry* **2000**, *48*, 53–69. [CrossRef]

52. Salimon, C.; Davidson, E.; Victoria, R.; Melo, A. CO_2 flux from soil in pastures and forests in Southwestern Amazonia. *Glob. Chang. Biol.* **2004**, *10*, 833–843. [CrossRef]

53. Raich, J.W.; Potter, C.S.; Bhagawati, D. Interannual variability in global soil respiration, 1980–94. *Glob. Chang. Biol.* **2002**, *8*, 800–812. [CrossRef]

54. Wang, X.; Ma, M.; Li, X.; Song, Y.; Tan, J.; Huang, G.; Yu, W. Comparison of remote sensing based GPP models at an alpine meadow site. *J. Remote Sens.* **2012**, *16*.

55. Yang, Y.; Fang, J.; Ji, C.; Han, W. Above-and belowground biomass allocation in Tibetan grasslands. *J. Veg. Sci.* **2009**, *20*, 177–184. [CrossRef]

56. Piao, S.; Yin, G.; Tan, J.; Cheng, L.; Huang, M.; Li, Y.; Liu, R.; Mao, J.; Myneni, R.B.; Peng, S. Detection and attribution of vegetation greening trend in china over the last 30 years. *Glob. Chang. Biol.* **2015**, *21*, 1601–1609. [CrossRef] [PubMed]

57. Piao, S.; Luyssaert, S.; Ciais, P.; Janssens, I.A.; Chen, A.; Cao, C.; Fang, J.; Friedlingstein, P.; Luo, Y.; Wang, S. Forest annual carbon cost: A global-scale analysis of autotrophic respiration. *Ecology* **2010**, *91*, 652–661. [CrossRef] [PubMed]

58. Chapin, F.S., III; Matson, P.A.; Vitousek, P. *Principles of Terrestrial Ecosystem Ecology*; Springer Science & Business Media: Luxemburg, 2011.

59. Craine, J.; Tilman, D.; Wedin, D.; Reich, P.; Tjoelker, M.; Knops, J. Functional traits, productivity and effects on nitrogen cycling of 33 grassland species. *Funct. Ecol.* **2002**, *16*, 563–574. [CrossRef]

60. Mahecha, M.D.; Reichstein, M.; Carvalhais, N.; Lasslop, G.; Lange, H.; Seneviratne, S.I.; Vargas, R.; Ammann, C.; Arain, M.A.; Cescatti, A. Global convergence in the temperature sensitivity of respiration at ecosystem level. *Science* **2010**, *329*, 838–840. [CrossRef] [PubMed]

61. Hirota, M.; Zhang, P.; Gu, S.; Du, M.; Shimono, A.; Shen, H.; Li, Y.; Tang, Y. Altitudinal variation of ecosystem CO_2 fluxes in an alpine grassland from 3600 to 4200 m. *J. Plant Ecol.* **2009**, *2*, 197–205. [CrossRef]

62. Geng, Y.; Wang, Y.; Yang, K.; Wang, S.; Zeng, H.; Baumann, F.; Kuehn, P.; Scholten, T.; He, J.-S. Soil respiration in Tibetan alpine grasslands: Belowground biomass and soil moisture, but not soil temperature, best explain the large-scale patterns. *PLoS ONE* **2012**, *7*, e34968. [CrossRef] [PubMed]

63. Jiang, J.; Shi, P.; Zong, N.; Fu, G.; Shen, Z.; Zhang, X.; Song, M. Climatic patterns modulate ecosystem and soil respiration responses to fertilization in an alpine meadow on the Tibetan Plateau, China. *Ecol. Res.* **2015**, *30*, 3–13. [CrossRef]

64. Zhao, J.; Luo, T.; Li, R.; Li, X.; Tian, L. Grazing effect on growing season ecosystem respiration and its temperature sensitivity in alpine grasslands along a large altitudinal gradient on the central Tibetan Plateau. *Agric. For. Meteorol.* **2016**, *218*, 114–121. [CrossRef]

65. Wagle, P.; Kakani, V.G. Confounding effects of soil moisture on the relationship between ecosystem respiration and soil temperature in switchgrass. *Bioenergy Res.* **2014**, *7*, 789–798. [CrossRef]

66. Chen, Q.; Wang, Q.; Han, X.; Wan, S.; Li, L. Temporal and spatial variability and controls of soil respiration in a temperate steppe in Northern China. *Glob. Biogeochem. Cycle* **2010**, *24*. [CrossRef]

67. Dornbush, M.E.; Raich, J.W. Soil temperature, not aboveground plant productivity, best predicts intra-annual variations of soil respiration in central Iowa grasslands. *Ecosystems* **2006**, *9*, 909–920. [CrossRef]

68. Wan, S.; Norby, R.J.; Ledford, J.; Weltzin, J.F. Responses of soil respiration to elevated CO$_2$, air warming, and changing soil water availability in a model old-field grassland. *Glob. Chang. Biol.* **2007**, *13*, 2411–2424. [CrossRef]

69. Davidson, E.; Belk, E.; Boone, R.D. Soil water content and temperature as independent or confounded factors controlling soil respiration in a temperate mixed hardwood forest. *Glob. Chang. Biol.* **1998**, *4*, 217–227. [CrossRef]

70. HoÈgberg, P.; Nordgren, A.; Buchmann, N.; Taylor, A.F.; Ekblad, A.; HoÈgberg, M.N.; Nyberg, G.; Ottosson-LoÈfvenius, M.; Read, D.J. Large-scale forest girdling shows that current photosynthesis drives soil respiration. *Nature* **2001**, *411*, 789–792. [CrossRef] [PubMed]

71. Yang, Y.; Fang, J.; Ma, W.; Guo, D.; Mohammat, A. Large-scale pattern of biomass partitioning across China's grasslands. *Glob. Ecol. Biogeogr.* **2010**, *19*, 268–277. [CrossRef]

72. Oleson, K.W.; Lawrence, D.M.; Gordon, B.; Flanner, M.G.; Kluzek, E.; Peter, J.; Levis, S.; Swenson, S.C.; Thornton, E.; Feddema, J. *Technical Description of Version 4.0 of the Community land Model (CLM)*; National Center for Atmospheric Research: Boulder, CO, USA, 2010.

73. Schimel, D.S.; Participants, V.; Braswell, B. Continental scale variability in ecosystem processes: Models, data, and the role of disturbance. *Ecol. Monogr.* **1997**, *67*, 251–271. [CrossRef]

74. Parton, W.J.; Hartman, M.; Ojima, D.; Schimel, D. Daycent and its land surface Submodel: Description and testing. *Glob. Planet. Chang.* **1998**, *19*, 35–48. [CrossRef]

75. Cramer, W.; Bondeau, A.; Woodward, F.I.; Prentice, I.C.; Betts, R.A.; Brovkin, V.; Cox, P.M.; Fisher, V.; Foley, J.A.; Friend, A.D. Global response of terrestrial ecosystem structure and function to CO$_2$ and climate change: Results from six dynamic global vegetation models. *Glob. Chang. Biol.* **2001**, *7*, 357–373. [CrossRef]

76. Wang, T.; Ciais, P.; Piao, S.; Ottle, C.; Brender, P.; Maignan, F.; Arain, A.; Gianelle, D.; Gu, L.; Lafleur, P. Controls on winter ecosystem respiration at mid-and high-latitudes. *Biogeoscience* **2010**, *7*. [CrossRef]

77. Mielnick, P.C.; Dugas, W.A. Soil CO$_2$ flux in a tallgrass prairie. *Soil Biol. Biochem.* **2000**, *32*, 221–228. [CrossRef]

78. Liu, X.; Wan, S.; Su, B.; Hui, D.; Luo, Y. Response of soil CO$_2$ efflux to water manipulation in a tallgrass prairie ecosystem. *Plant Soil* **2002**, *240*, 213–223. [CrossRef]

79. Fernández-Martínez, M.; Vicca, S.; Janssens, I.A.; Campioli, M. Nutrient availability as the key regulator of global forest carbon balance. *Nat. Clim. Chang.* **2014**, *4*, 471–476. [CrossRef]

80. Xiao, X.; Hollinger, D.; Aber, J.; Goltz, M.; Davidson, E.A.; Zhang, Q.; Moore, B. Satellite-based modeling of gross primary production in an evergreen Needleleaf forest. *Remote Sens. Environ.* **2004**, *89*, 519–534. [CrossRef]

81. Wu, C.; Niu, Z.; Gao, S. Gross primary production estimation from Modis data with vegetation index and photosynthetically active radiation in maize. *J. Geophys. Res. Atmos.* **2010**, *115*. [CrossRef]

82. Yuste, J.C.; Janssens, I.; Carrara, A.; Meiresonne, L.; Ceulemans, R. Interactive effects of temperature and precipitation on soil respiration in a temperate maritime pine forest. *Tree Physiol.* **2003**, *23*, 1263–1270. [CrossRef]

83. Amos, B.; Arkebauer, T.J.; Doran, J.W. Soil surface fluxes of greenhouse gases in an irrigated maize-based agroecosystem. *Soil Sci. Soc. Am. J.* **2005**, *69*, 387–395. [CrossRef]